

Vapor driven sublacustrine vents in Yellowstone Lake, Wyoming

Andrew P.G. Fowler^{1,*}, Chunyang Tan¹, Christie Cino¹, Peter Scheuermann¹, Michael W.R. Volk¹, W. C. Pat Shanks III², William E. Seyfried Jr¹.

¹ *Department of Earth Sciences, University of Minnesota, Minneapolis, MN 55455, USA*

² *U.S. Geological Survey, Denver Federal Center, MS 973, Denver, CO 80225-0046, USA*

SAMPLING AND ANALYTICAL METHODS

Pressurized fluid samples were obtained using a gas tight sampler (Wu et al., 2011) affixed to the remotely operated vehicle (ROV) “Yogi” and support vessel R/V Annie that are owned and operated by the Global Foundation for Ocean Exploration. The gas-tight (isobaric) sampling system is constructed entirely of titanium and has real-time temperature monitoring capability. The isobaric capability means that lake-bottom pressure is maintained up to the point of subsampling at the surface, facilitating acquisition and analysis of gas-rich fluid samples from vents. In 2016, a polycarbonate cup was fixed to the fluid sampling snorkel and placed immediately above the vent orifice to focus vent fluid into the gas tight sampling device. The sampling apparatus attached to the snorkel was re-designed in 2017 as a titanium push sampler with a built-in filtration system that could be inserted into vent orifices to minimize entrainment of ambient lake water (Figure S1). Sediment cores (5 to 19 cm long) were obtained from within and adjacent to vent orifices in 2017 using 2-inch diameter titanium tubes pushed into the substrate using the manipulator arm of the ROV. Sediment samples were transferred to polycarbonate sleeves and immediately frozen upon recovery to minimize oxidation. Sediment cores were

processed in the National Science Foundation (NSF) funded LaCore facility at the University of Minnesota (UMN)

Fluid samples were analyzed in triplicate for Cl and SO₄ using a Thermo Dionex ICS 5000 ion chromatography (IC) system, and Ca, K, Mg, Na, and Si using a Thermo Scientific iCAP 6500 duo ICP-OES at the UMN Department of Earth Sciences aqueous geochemistry lab. Sample replicates agreed within 1% relative standard deviation (%RSD) for IC, 7% for ICP-OES, and multi-element standards at 5, 10, 20 and 40X dilutions analyzed in triplicate agreed within 2% RSD. CO₂ was analyzed using gas chromatography verified using a commercial multi-gas standard. Sample aliquots for H₂S were transferred to evacuated amber bottles containing zinc acetate. The resulting zinc sulfide was collected on filter paper and dissolved in 6 molar oxygen-free HCl. The produced H₂S was transported using N₂ to an AgNO₃ solution where Ag₂S was formed, aged for a minimum of 3 hours, and subsequently filtered, dried and analyzed gravimetrically. Three tests using synthetic zinc sulfide had reproducibility within 7% for the Ag₂S gravimetric method. SO₄ was determined by analyzing the filtrate from the zinc acetate solution.

Stable isotopes of hydrogen and oxygen of fluid samples were measured at the USGS in Denver, Colorado. Simultaneous analysis of δD and $\delta^{18}\text{O}$ of water samples was carried out with a Picarro L2130-*i* water isotope analyzer that uses cavity ring-down spectroscopy with an IR laser diode to measure absorption by isotopic species. The hydrogen and oxygen isotope ratios are reported using standard δ notation relative to Vienna Standard Mean Ocean Water (VSMOW). Sample values were normalized using laboratory working standards that had been calibrated using

certified VSMOW2 and SLAP2 reference materials. Precision of replicate analyses gave standard deviations of $\leq 0.5\text{‰}$ for δD and $\leq 0.10\text{‰}$ for $\delta^{18}\text{O}$. Mean values determined for NIST reference material 8536 (GISP) that was analyzed as a check standard were within 0.1 and 0.5‰ of mean certified $\delta^{18}\text{O}$ (-24.78) and δD (-189.5) values, respectively.

Vent substrate mineralogy was analyzed by X-Ray diffraction using a Rigaku MiniFlex instrument at UMN. Samples were prepared by decantation (Poppe et al., 2001). Sample separates were analyzed untreated, treated with ethylene glycol for 24 hours, and heated to 550 °C for 2 hours. Samples were analyzed at a scan speed of 1°/minute, sampling width of 0.02° and 2 θ scan angle between 4 and 65° using a cobalt K α source. The coarse sediment residue after decantation was preserved and examined with a scanning electron microscope at LaCORE and mineralogy was confirmed using spot EDS analysis with a minimum 1-minute counting time. XRD and SEM results are provided as supplemental data figures 1 through 3.

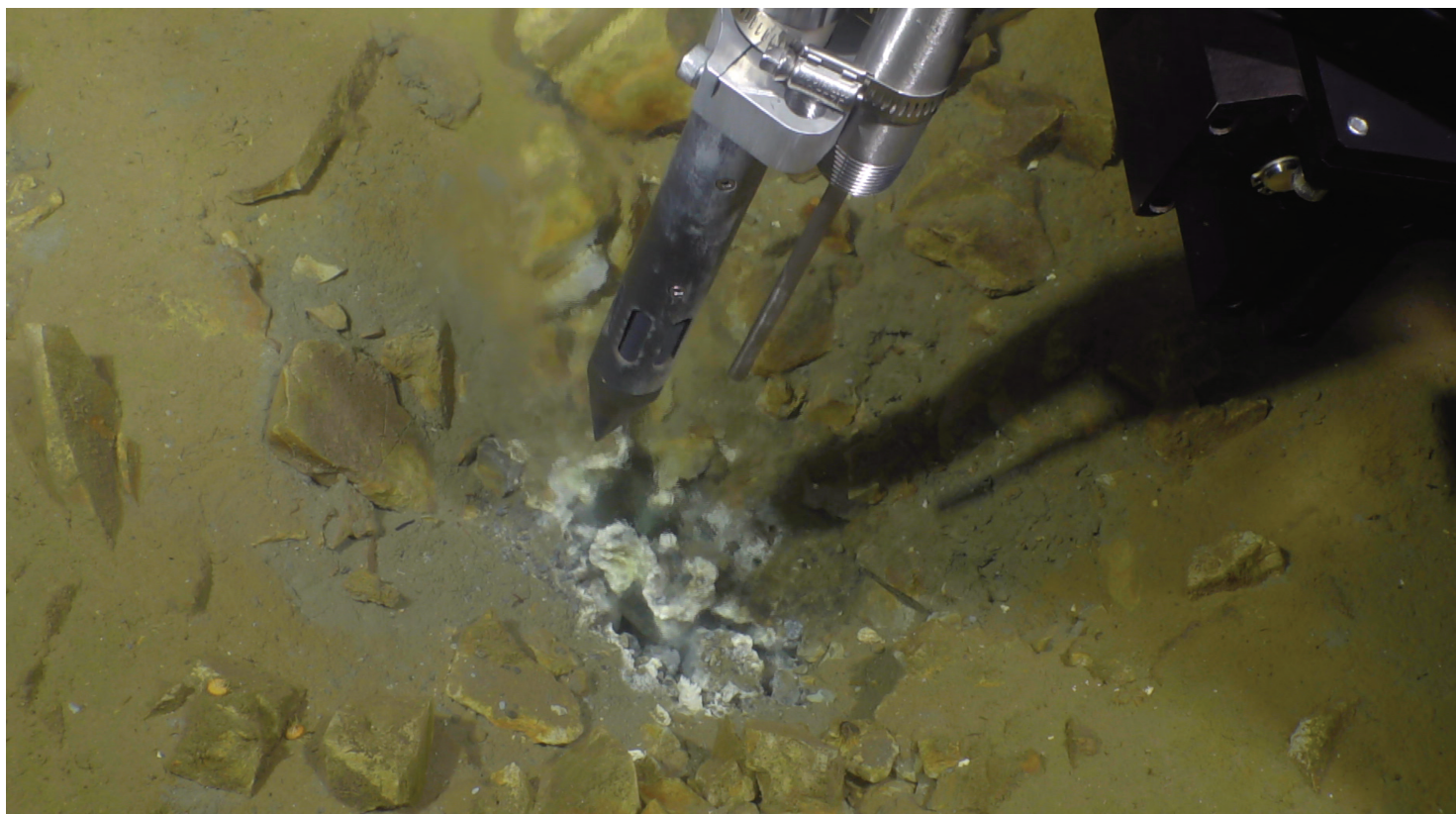
Pyrrhotite occurrence was determined from hysteresis loops measured on a Princeton Instruments vibrating sample magnetometer and zero-field low temperature cycling (300 K – 10 K) of a room temperature saturating isothermal remnant magnetization (RTSIRM), acquired in a 2.5 T field on a Quantum Design Magnetic Property Measurement System (MPMS) at the Institute for Rock Magnetism at UMN. The cooling rate and step size was 5K/min. In the RTSIRM data, a drop in magnetization at ≈ 30 kelvin (Supplemental data figure 5) is typical for the Besnus transition in monoclinic pyrrhotite (Besnus and Meyer, 1964; Volk et al., 2016). The saturation magnetization (M_s) determined from hysteresis loop data after correction for paramagnetic contributions was used to qualitatively estimate the ferrimagnetic component in

samples. The samples have a large paramagnetic component, visible in the linear positive slope at high magnetic fields. Assuming no other ferrimagnetic minerals are present in the samples, the amount of monoclinic pyrrhotite can be determined by relating M_s of the sample with that of pyrrhotite. However, some samples showed signs of different magnetic mineral, magnetite, for example YL17U03 – 2 cm, which shows signs of the magnetite Verwey transition (≈ 120 K) in the RTSIRM data. Thus, estimates for pyrrhotite content are a maximum for the monoclinic pyrrhotite variety. After correction for sample volumes that were concentrated from dominantly kaolinite substrate, pyrrhotite occurrence accounts for < 0.5 weight percent for all samples.

REFERENCES CITED

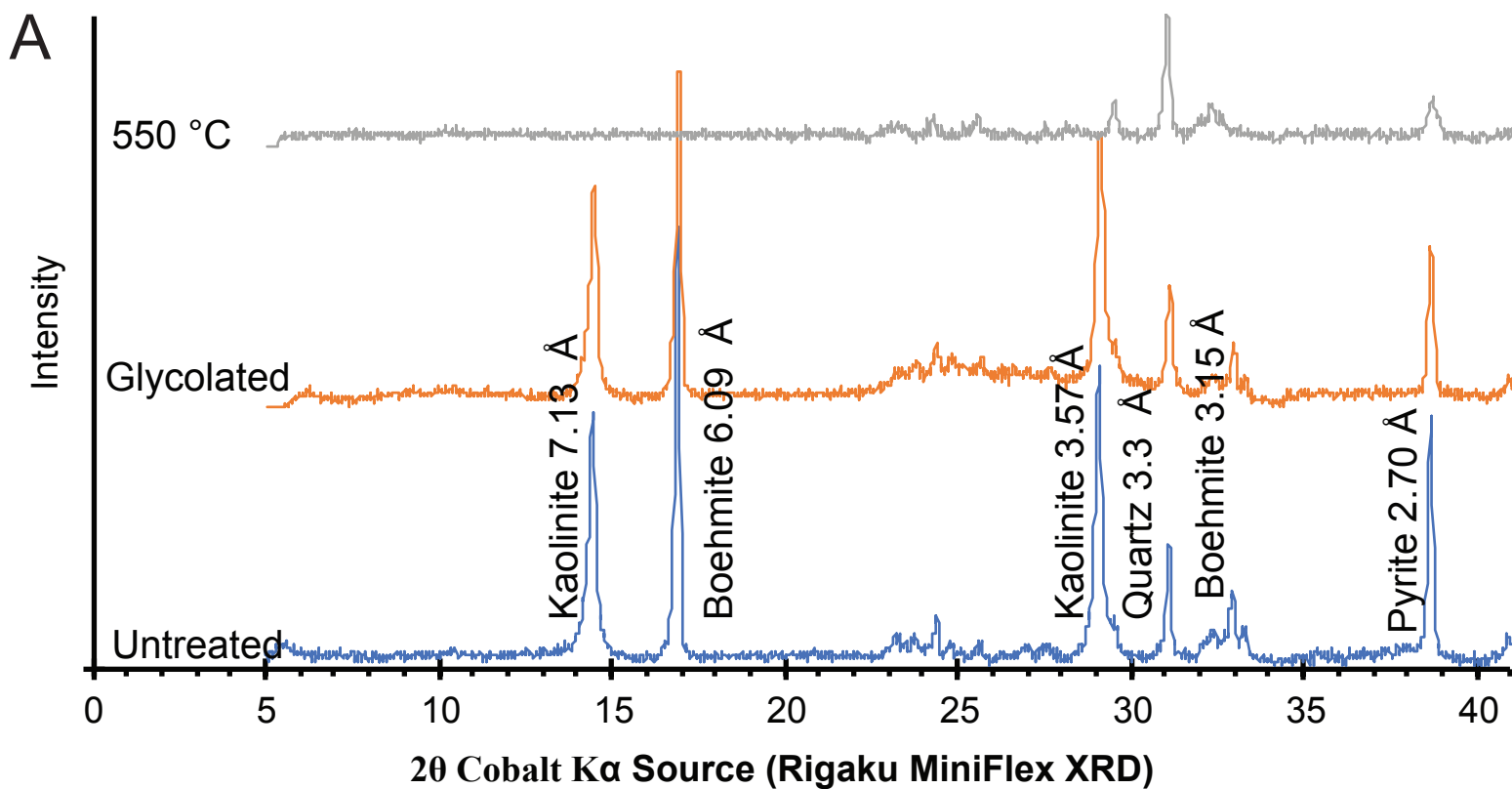
- Besnus, M. J., and Meyer, A. J., 1964, Nouvelles données expérimentales sur le magnétisme de la pyrrhotine naturelle.: Proceedings of the International Conference on Magnetism, v. 20, p. 507-511.
- Poppe, L. J., Paskevich, V. F., Hathaway, J. C., and Blackwood, D. S., 2001, A laboratory manual for X-ray powder diffraction: U.S. Geological Survey Open-File Report, v. 01-041, p. 88.
- Volk, M. W. R., Gilder, S. A., and Feinberg, J. M., 2016, Low-temperature magnetic properties of monoclinic pyrrhotite with particular relevance to the Besnus transition: Geophysical Journal International, v. 207, no. 3, p. 1783-1795.
- Wu, S.-J., Yang, C.-J., Pester, N. J., and Chen, Y., 2011, A New Hydraulically Actuated Titanium Sampling Valve for Deep-Sea Hydrothermal Fluid Samplers: IEEE Journal of Oceanic Engineering, v. 36, no. 3, p. 462-469.

Video DR1 (brief footage of gas bubbles exiting a sublacustrine hydrothermal vent)

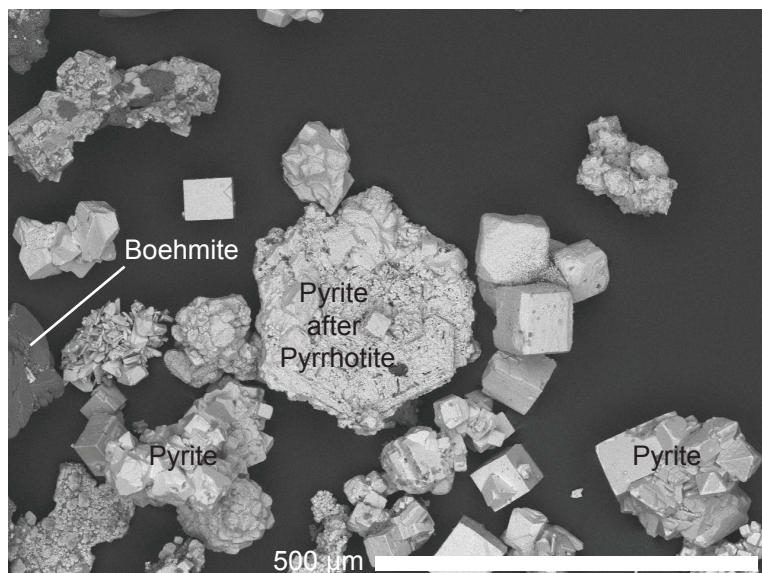


Supplemental Figure S1. Vent YL17F01. Cone-tipped titanium fluid sampler approximately 3 cm diameter being inserted into a 174 °C shimmering fluid vent.

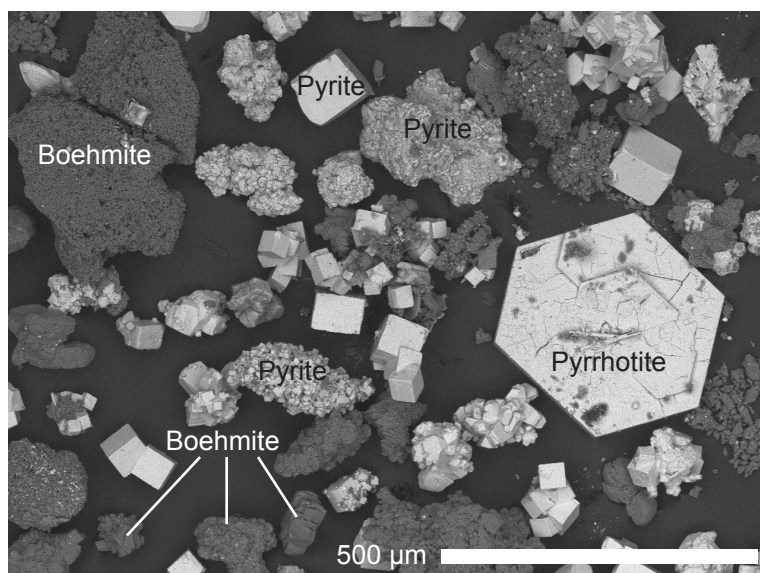
Figure S2: (A) X-ray diffraction (XRD) results for the clay-sized fraction and (B, C) scanning electron microscope (SEM) images of the remaining particles for sediment 2 cm from the top of core YL17U04, collected 1 m from a vent throat.



B

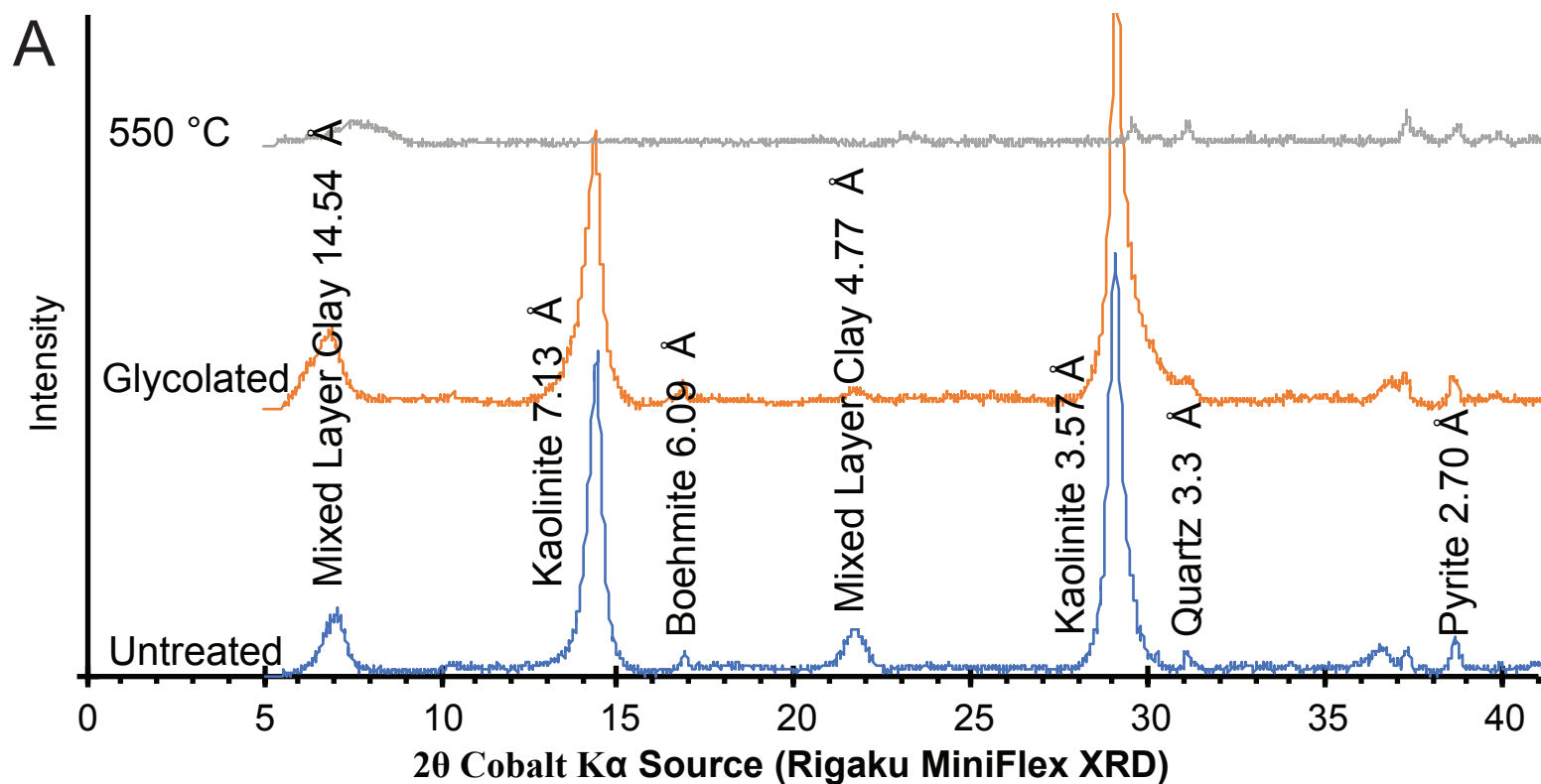


C

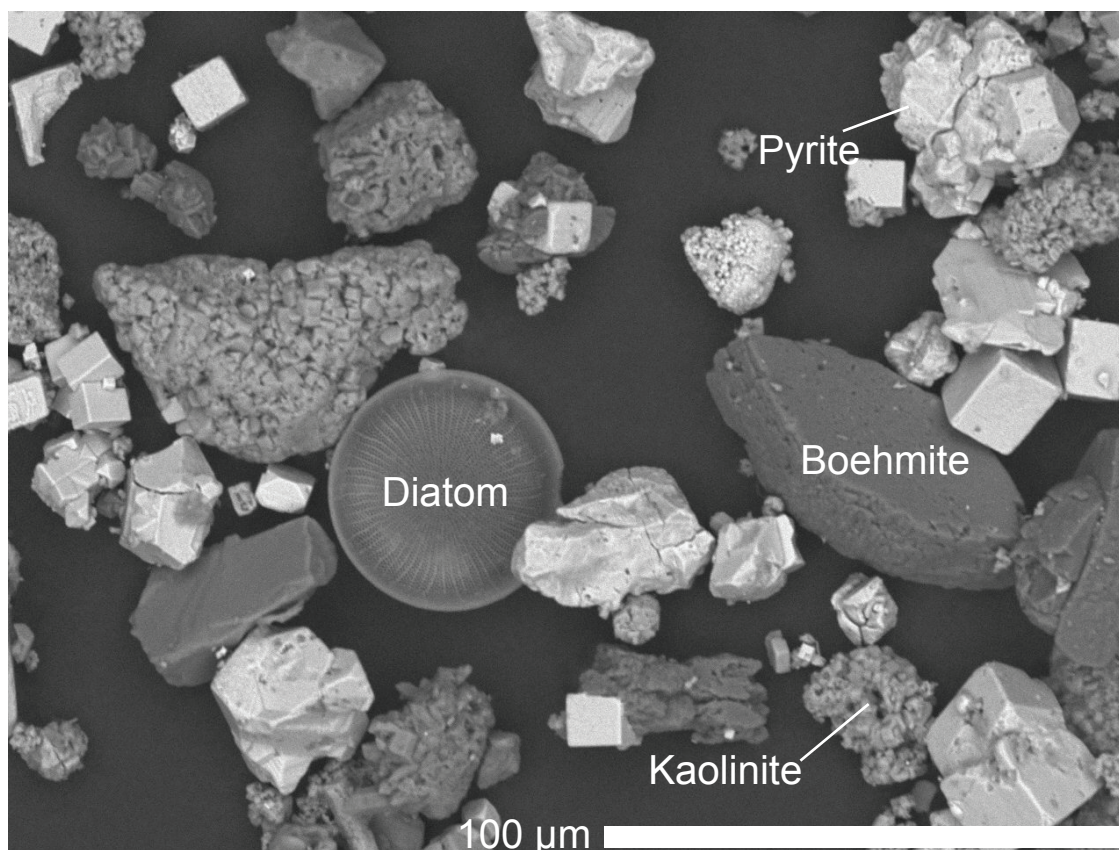


Coarse fraction SEM image, LaCore, UMN, funded by NSF

Figure S3: (A) XRD results for the clay-sized fraction and (B) SEM images of the remaining particles for sediment 14 cm from the top of core YL17U04, collected 1 m from a vent throat.

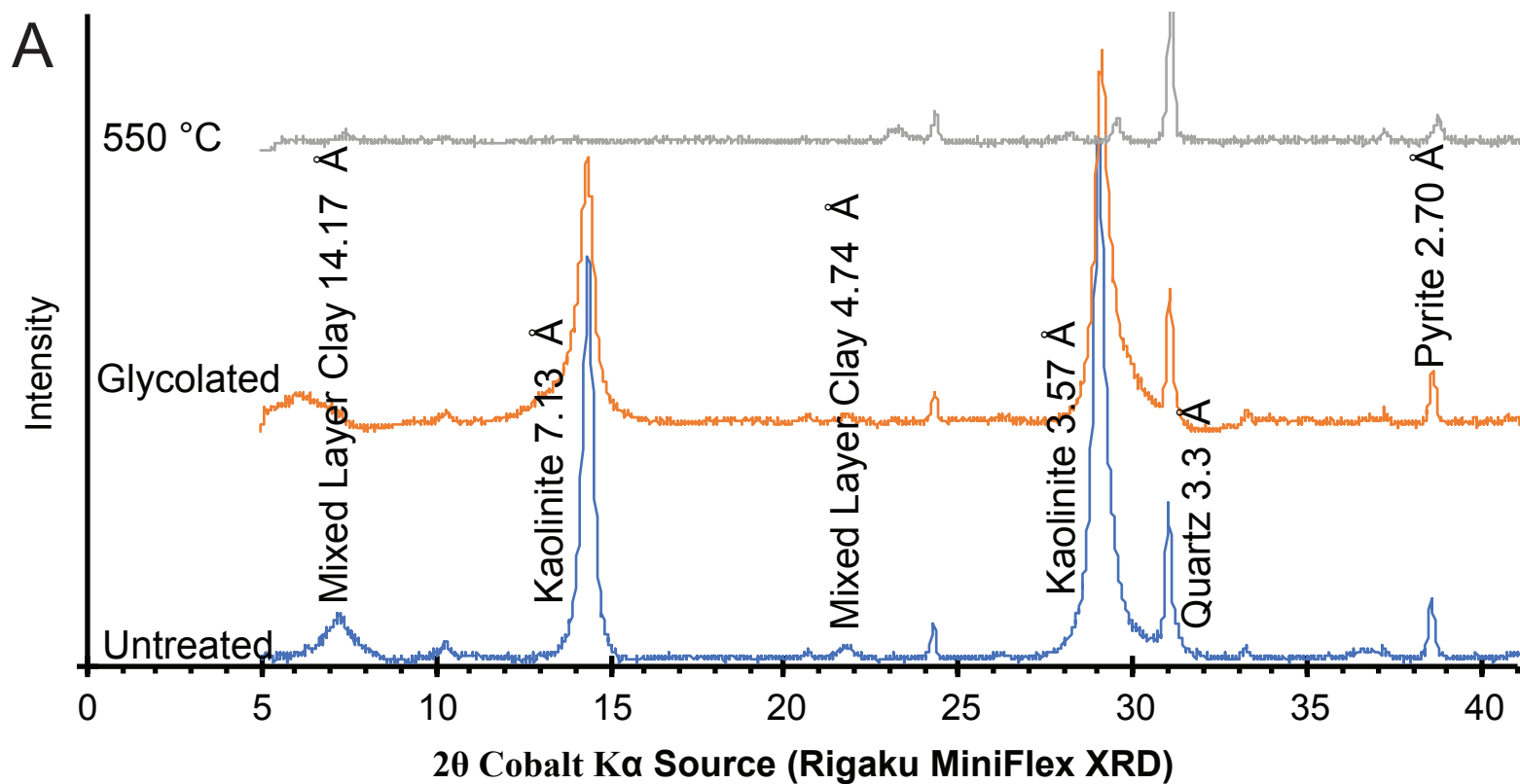


B

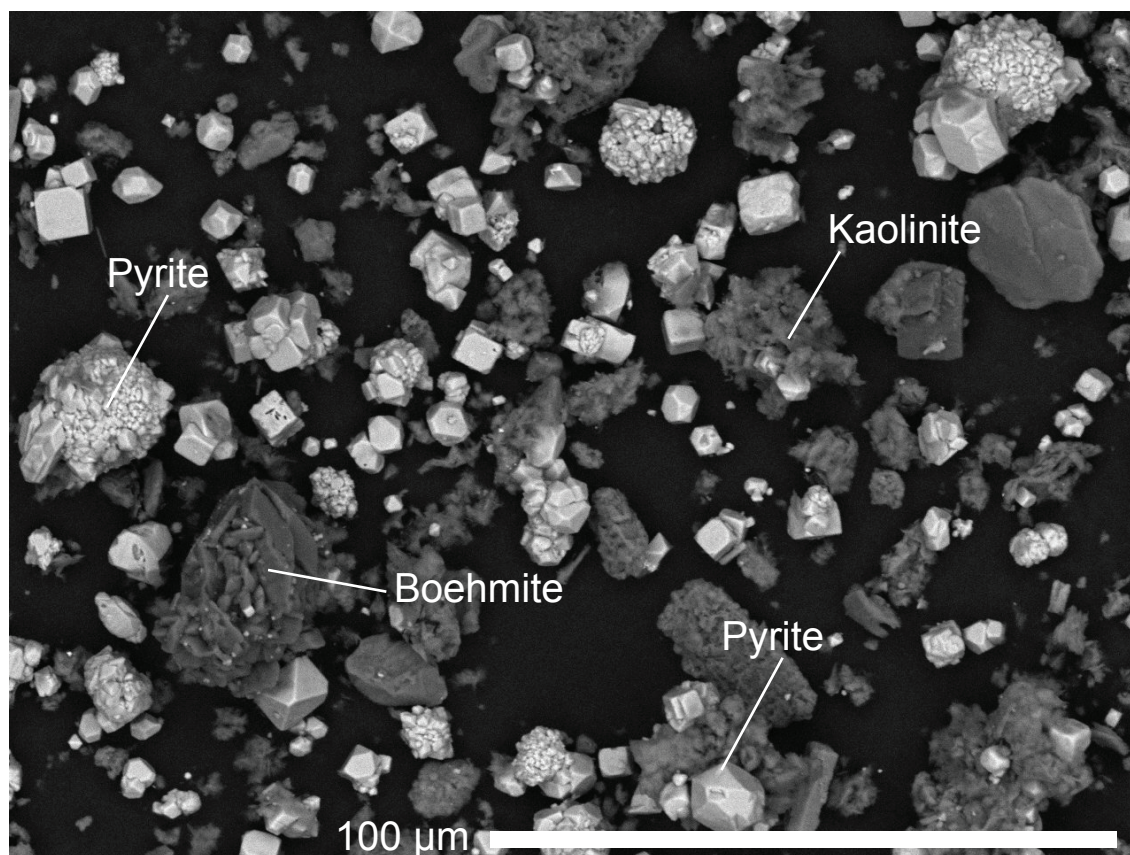


Coarse fraction SEM image, LaCore, UMN, funded by NSF

Figure S4: (A) XRD results for the clay-sized fraction and (B) SEM images of the remaining particles for sediment 14 cm from the top of core YL17U03, collected from a vent throat.



B



Coarse fraction SEM image, LaCore, UMN, funded by NSF

